EXAFS, x-ray diffraction, and reverse Monte Carlo simulations of an amorphous $Ni_{60}Ti_{40}$ alloy produced by mechanical alloying

K. D. Machado,* J. C. de Lima,† C. E. M. de Campos, T. A. Grandi, and D. M. Trichês
Departamento de Física, Universidade Federal de Santa Catarina, 88040-900 Florianópolis, SC, Brazil
(Received 19 March 2002; revised manuscript received 5 July 2002; published 16 September 2002)

The local atomic order of an amorphous $Ni_{60}Ti_{40}$ alloy produced by mechanical alloying was studied by extended x-ray absorption fine structure (EXAFS) and x-ray diffraction (XRD) techniques. The experimental total structure factor derived from the XRD measurements was simulated by using the reverse Monte Carlo (RMC) method. This simulation was used to compute the $\mathcal{S}^c_{\text{Ni-Ni}}(K)$, $\mathcal{S}^c_{\text{Ni-Ti}}(K)$, and $\mathcal{S}^c_{\text{Ti-Ti}}(K)$ partial structure factors and to infer a three-dimensional structure for this alloy. The coordination numbers and interatomic distances for the first neighbors obtained from EXAFS and RMC showed a good agreement. The bond-angle distributions derived from the structure obtained by RMC simulations give evidence that the structure of amorphous $Ni_{60}Ti_{40}$ alloy contains distorted trigonal-prismatic units. The calculated Warren chemical short-range order parameter showed a local chemical order similar to that one found in the solid solutions and in the Ni_3Ti compound and different of that found in the NiTi compound.

DOI: 10.1103/PhysRevB.66.094205 PACS number(s): 61.10.Eq, 61.10.Ht, 61.43.Bn, 05.10.Ln

I. INTRODUCTION

Since the discovery that mechanical alloying (MA)[1] is an efficient means for synthesizing crystalline[2] and amorphous[3] materials, as well as stable and metastable solid solutions,[4,5] some researchers have turned their attention to this technique. MA has also been used to produce materials with nanometer sized grains and alloys whose components have large differences in their melting temperatures, such as iron ($T_m = 1535\,^\circ$C) and selenium ($T_m = 217\,^\circ$C) and are thus difficult to produce using techniques based on melting.

From a structural point of view, both the crystalline elemental metal powders with nanometer sized grains, obtained via ball-milling, and the crystalline alloys synthesized by MA can be regarded as being made up of two components, one crystalline, with grains of dimensions of a few nanometers, that preserves the structure of bulk crystal, and one interfacial, composed by defects centers.[6] The interfacial component arises only when grain size is reduced to a few nanometers.

In the last two decades, a large number of publications have appeared describing the properties of amorphous alloys produced by MA. Among them, very few deal with atomic structure determination. This is probably due to the difficulty of extracting structural information from the radial distribution functions deduced from extended x-ray absorption fine structure (EXAFS), x-ray diffraction (XRD), and neutron diffraction measurements.

The reverse Monte Carlo (RMC) simulation[7–9] is a method for structural modeling based directly on experimental data. In order to investigate the local structure of amorphous alloys, the total structure factor $\mathcal{S}(K)$ or radial distribution functions derived from XRD or neutron measurements are used as input data. There are in the literature several papers reporting results about the application of the RMC method to investigate the structures of amorphous alloys.[10–14]

In this paper, the local atomic structure of the amorphous $Ni_{60}Ti_{40}$ (a-$Ni_{60}Ti_{40}$) alloy produced by MA has been investigated by combining the EXAFS and XRD techniques with RMC simulations[7–9] of the experimental total structure factor $\mathcal{S}^e(K)$ derived from the x-ray measurement.

II. THEORETICAL FUNDAMENTALS FOR RMC SIMULATIONS

A. Total and partial structure factors and reduced distribution functions

The total Faber-Ziman[15] structure factor $\mathcal{S}(K)$ is obtained from the intensity per atom $I_a(K)$ using the equation

$$\mathcal{S}(K) = \frac{I_a(K) - \langle f^2(K)\rangle}{\langle f(K)\rangle^2},$$

$$\mathcal{S}(K) = \sum_\alpha \sum_\beta w_{\alpha,\beta}(K)[\mathcal{S}_{\alpha,\beta}(K) - 1], \tag{1}$$

where $K = 4\pi \sin\theta/\lambda$, λ is the wavelength of the scattered radiation, 2θ is the diffraction angle, $\mathcal{S}_{\alpha,\beta}(K)$ are the partial structure factors, $w_{\alpha,\beta}(K)$ is given by

$$w_{\alpha,\beta}(K) = \frac{c_\alpha c_\beta f_\alpha(K) f_\beta(K)}{\langle f(K)\rangle^2}, \tag{2}$$

and

$$\langle f^2(K)\rangle = \sum_\alpha c_\alpha f_\alpha^2(K),$$

$$\langle f(K)\rangle^2 = \left[\sum_\alpha c_\alpha f_\alpha(K)\right]^2.$$

Here, $f_\alpha(K) = f_0(K) + f'(\lambda) + if''(\lambda)$ is the atomic scattering factor, $f'(\lambda)$ and $f''(\lambda)$ are the anomalous dispersion terms which depend of the wavelength of radiation, and c_α is the concentration of atoms of type α. The total reduced dis-

tribution function $G(r)$ is related to the total structure factor $\mathcal{S}(K)$ through the Fourier transform

$$G(r)=\frac{2}{\pi}\int_0^\infty K[\mathcal{S}(K)-1]\sin(Kr)dK, \tag{3}$$

while the partial reduced distribution functions $G_{\alpha,\beta}(r)$ are related to the partial structure factors $\mathcal{S}_{\alpha,\beta}(K)$ by means of the Fourier transform

$$G_{\alpha,\beta}(r)=\frac{2}{\pi}\int_0^\infty K[\mathcal{S}_{\alpha,\beta}(K)-1]\sin(Kr)dK. \tag{4}$$

From $G_{\alpha,\beta}(r)$ the partial radial distribution function $\mathrm{RDF}_{\alpha,\beta}(r)$ can be calculated by

$$\mathrm{RDF}_{\alpha,\beta}(r)=4\pi\rho_0 r^2+rG_{\alpha,\beta}(r). \tag{5}$$

Interatomic distances are obtained from the maxima of $G_{\alpha,\beta}(r)$, while coordination numbers are calculated by integrating the peaks of $\mathrm{RDF}_{\alpha,\beta}(r)$.

B. The RMC method

The basic idea and the algorithm of standard RMC method are described elsewhere.[7–9] Applications of this method to polymeric,[16] crystalline,[17] and amorphous[10,18–23] materials are described in the literature. In order to simulate the atomic structure of an amorphous alloy by the RMC method, it is necessary to use as input data one or more experimental total structure factor $\mathcal{S}^e(K)$, the weights $w_{\alpha,\beta}(K)$ given by Eq. (2), the density (in atoms/Å^3) and the chemical composition of the alloy. The $\mathcal{S}^e(K)$ can be extracted from neutron diffraction or x-ray diffraction (XRD) measurements. The EXAFS Fourier-filtered first shell function $\chi(k)$ can also be used. In the RMC procedure, a three-dimensional arrangement of atoms with the same density and chemical composition of the alloy is placed into a cell (usually cubic) with periodic boundary conditions and the $G^c_{\alpha,\beta}(r)$ functions corresponding to it are directly calculated through

$$G^c_{\alpha,\beta}(r)=\frac{n^c_{\alpha,\beta}(r)}{4\pi\rho_0 r^2\Delta r},$$

where $n^c_{\alpha,\beta}(r)$ is the number of atoms at a distance between r and $r+\Delta r$ from the central atom, averaged over all atoms. By allowing the atoms to move (one at each time) inside the cell, the $G^c_{\alpha,\beta}(r)$ functions can be changed and, as a consequence, the partial and total calculated structure factors $\mathcal{S}_{\alpha,\beta}(K)$ and $\mathcal{S}^c(K)$, calculated using Eqs. (1) and (4), are changed. Thus, $\mathcal{S}^c(K)$ is compared to $\mathcal{S}^e(K)$ in order to minimize the differences between them. The function to be minimized is

$$\psi^2=\frac{1}{\delta}\sum_{i=1}^{m}[\mathcal{S}^c(K_i)-\mathcal{S}^e(K_i)]^2, \tag{6}$$

where the sum is over m experimental points and δ is related to the experimental error in $\mathcal{S}^e(K)$. If the movement decreases ψ^2, it is always accepted. If it increases ψ^2, it is accepted with a probability given by $\exp(-\Delta\psi^2/2)$; otherwise it is rejected. As this process is iterated ψ^2 decreases until it reaches an equilibrium value. Thus, the atomic configuration corresponding to equilibrium should be consistent with the experimental total structure factor within the experimental error. By using the $G^c_{\alpha,\beta}(r)$ and $\mathcal{S}^c_{\alpha,\beta}(K)$ functions corresponding to the final three-dimensional structure, the coordination numbers and interatomic distances can be calculated. In addition, the bond-angle distributions can also be determined.

III. EXPERIMENTAL PROCEDURE

Binary mixtures of high-purity elemental powders of nickel (Merck 99.5%, particle size <10 μm) and titanium (BDH 99.5%, particle size <10 μm) with nominal composition $Ni_{60}Ti_{40}$ were sealed together with several steel balls into a cylindrical steel vial under an argon atmosphere. The ball-to-powder weight ratio was 5:1. A Spex Mixer/Mill model 8000 was used to perform MA at room temperature. The mixture was continuously milled for 9 h. A ventilation system was used to keep the vial temperature close to room temperature. The composition of the as-milled powder was measured using the energy dispersive spectroscopy (EDS) technique, giving a composition of 39.79 and 60.21 at. % of Ti and Ni, respectively. Impurity traces were not observed. The XRD pattern was recorded in a powder Siemens diffractometer equipped with a graphite monochromator, using the CuK_α line ($\lambda=1.5418$ Å). The total structure factor $\mathcal{S}^e(K)$ was computed from the XRD pattern after corrections for polarization, absorption, and inelastic scattering, following the procedure described by Wagner.[24] The f' and f'' values were taken from a table compiled by Sasaki.[25]

The EXAFS experiments were carried out on the D04B beam line of the Laboratório Nacional de Luz Síncrotron (LNLS) in Campinas, Brazil,[26] using a channel cut monochromator (Si 111), two ionization chambers as detectors and a 1 mm entrance slit. This yielded a resolution of about 1.6 eV at the Ti K edge (4966 eV) and 3.9 eV at the Ni K edge (8333 eV). All data were taken at room temperature in the transmission mode. The energy and current of the storage ring were 1.37 GeV and 120 mA, respectively.

IV. RESULTS AND DISCUSSION

A. EXAFS measurements

The measured EXAFS spectra for a-$Ni_{60}Ti_{40}$ alloy were analyzed using standard data reduction procedures[27] with WINXAS97 software:[28] deglitching, background correction, normalization, set E_0, conversion to k space, smooth K-shell absorption background $\mu_0(k)$, extraction of the EXAFS signal $\chi(k)$ which is the oscillatory part of the absorption coefficient, k weighting, window functions (square, Gaussian, Bessel, Hanning, etc.), Fourier transform (FT) of $\chi(k)$ to real space (real and imaginary parts and FT magnitude), back FT to k space to obtain the Fourier-filtered first shell, extraction of phases and amplitudes, fit and simulation of the Fourier-

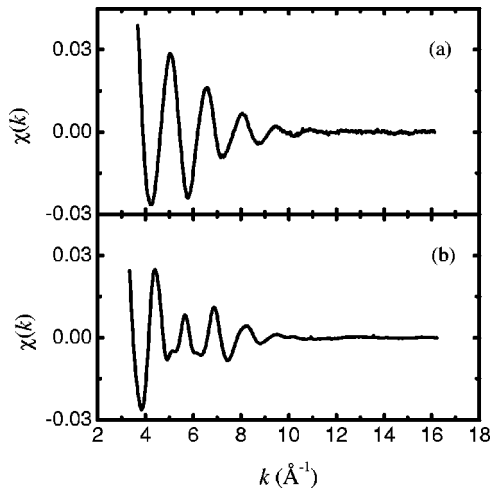

FIG. 1. Experimental EXAFS spectra: (a) at the Ni *K* edge and (b) at the Ti *K* edge.

filtered first shell by using the single scattering formula of Stern *et al.*[29] for Gaussian distributions or by using the FEFF method, etc.

Figure 1 shows the EXAFS oscillations $\chi(k)$ above the Ni and Ti *K* edges. The oscillations $\chi(k)$ on the Ni and Ti *K* edges contain structural data about the Ni-Ni and Ni-Ti pairs and Ti-Ni and Ti-Ti pairs, respectively. In order to extract these structural data, the signals $\chi(k)$ were weighted by a Bessel window function within the ranges $k = 3.9–14.1$ Å^{-1} and 3.6–13.9 Å^{-1} on the Ni and Ti edges, respectively, and their FT were then computed. Figure 2 shows their FT magnitudes. The FT magnitude curve at the Ti *K* edge (bottom curve) shows the shells corresponding to the Ti-Ni and Ti-Ti first neighbors partially separated while in the FT magnitude curve at the Ni *K* edge (top curve) the Ni-Ni and Ni-Ti shells are not separated. The FT magnitude curve is not a true radial distribution function, since the EXAFS oscillations are phase shifted by the atomic potentials (absorber and back-scatterer atoms), so that the positions of the peaks do not correspond to true distances. Usually, the peaks are shifted to low-*r* values by about 0.30–0.40 Å. In order to determine the coordination numbers and interatomic distances for the first neighbors, the FT's major shells in Fig. 2 (1.34–2.85 Å on the Ni edge, 1.05–3.39 Å on the Ti edge) were back transformed into *k* space. The Fourier-filtered first shells were then fitted by using Gaussian distributions to represent the homopolar (Ni-Ni and Ti-Ti) and heteropolar (Ni-Ti) bonds.[29] To fit them, the amplitude and phase shifts relative to the homopolar and heteropolar bonds were necessary. For the Ti-Ti bonds, the amplitude and phase shifts were obtained from Ti metal foil (purity better than 99.8%) used as standard at LNLS for energy calibration and its EXAFS signal $\chi(k)$ was treated in the same way than that one applied to the EXAFS signals $\chi(k)$ measured for the alloy. For the Ni-Ni bonds, the amplitude and phase shifts were obtained from Ni metal foil (purity better than 99.8%) also used as standard at LNLS for energy calibration and *ab initio* using the spherical waves method[30] and FEFF software. For the heteropolar bonds, the amplitude and phase shifts were calculated *ab initio* using the spherical waves method[30] and FEFF software. Figures. 3 and 4 show the experimental and the fitting results for the Fourier-filtered first shells on the Ni and Ti edges, respectively, and the structural parameters extracted from the fits are listed in Table I.

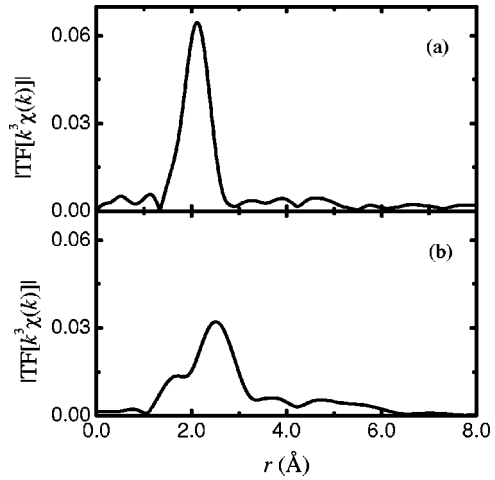

FIG. 2. Fourier transforms of experimental EXAFS spectra: (a) at the Ni *K* edge and (b) at the Ti *K* edge.

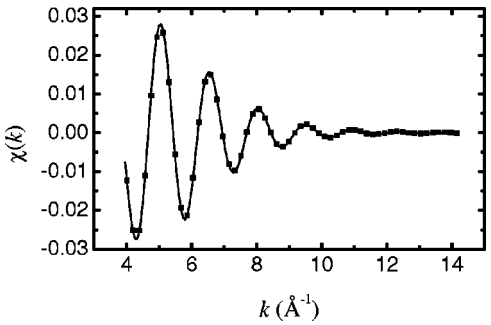

FIG. 3. Fourier-filtered first shell (full line) and its simulation (squares) for a-$Ni_{60}Ti_{40}$ at the Ni *K* edge.

As it can be seen in Table I, we have used two sub-shells for Ni-Ni, Ni-Ti, Ti-Ni, and Ti-Ti pairs. We started the fitting procedure using one shell for all pairs. This choice did not produce a good quality fit of Fourier-filtered first shells on the Ni and Ti edges. In addition to that, the well-known relations below were not verified in fitting EXAFS data:

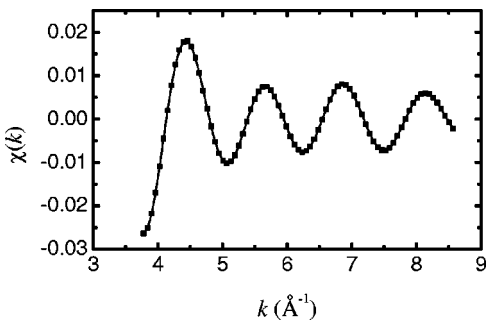

FIG. 4. Fourier-filtered first shell (full line) and its simulation (squares) for a-$Ni_{60}Ti_{40}$ at the Ti *K* edge.

TABLE I. Structural parameters for a-$Ni_{60}Ti_{40}$ alloy.

	EXAFS							
	Ni K edge				Ti K edge			
Bond type	Ni-Ni		Ni-Ti		Ti-Ni		Ti-Ti	
N	2.0	6.8	4.9	0.3	7.4	0.5	1.6	3.9
r (Å)	2.49	2.60	2.54	2.63	2.54	2.63	2.88	2.91
σ(Å$\times 10^{-2}$)	7.40	15.75	5.94	0.464	5.941	0.464	0.001	0.267
	RMC							
Bond type	Ni-Ni		Ni-Ti		Ti-Ni		Ti-Ti	
N	7.2 (3)		5.4 (2)		8.1 (2)		5.5 (1)	
r (Å)	2.58 (2)		2.52 (2)		2.52(2)		2.88 (2)	
	Ni_3Ti compound							
Bond type	Ni-Ni		Ni-Ti		Ti-Ni		Ti-Ti	
N	8.0		4.0		12.0		6.0	
r (Å)	2.55		2.55		2.55		3.60	
	NiTi compound							
Bond type	Ni-Ni		Ni-Ti		Ti-Ni		Ti-Ti	
N	6.0		8.0		8.0		6.0	
r (Å)	3.01		2.61		2.61		3.01	

[a]The numbers in parentheses are the errors in the last decimal place.

$$c_\alpha N_{\alpha,\beta} = c_\beta N_{\beta,\alpha},$$

$$r_{\alpha,\beta} = r_{\beta,\alpha},$$

$$\sigma_{\alpha,\beta} = \sigma_{\beta,\alpha}$$

where c_α is the concentration of atoms of type α, $N_{\alpha,\beta}$ is the number of β atoms located at a distance $r_{\alpha,\beta}$ around an α atom and $\sigma_{\alpha,\beta}$ is the half-width of the Gaussian. By considering two Ti-Ti subshells and one shell for the Ni-Ni and Ni-Ti pairs, the quality of the fits obtained was not improved. However, very good fits were achieved (see Figs. 3 and 4) considering two subshells for the Ni-Ni, Ni-Ti, Ti-Ni, and Ti-Ti pairs. Moreover, the relations above were satisfied. These results indicate that, although one subshell corresponding to the Ni-Ti and Ti-Ni pairs has a very small number of atoms, its contribution to the EXAFS fits is not negligible.

B. The RMC Simulations

In order to make the simulations we have considered a cubic cell with 4000 atoms (2400 Ni and 1600 Ti), $\delta = 0.01$, and an average density $\rho_0 = 6.957$ g/cm^3 $= 0.0771$ atoms/Å^3, which had been previously calculated.[31] In order to study the influence of the density value, we have changed it in the range up to $\pm 10\%$, but the best convergence of the ψ^2 parameter [see Eq. (6)] was reached for the value given above. The minimum distances between atoms were fixed at the beginning of the simulations to $r_{\text{Ni-Ni}} = 2.0$ Å, $r_{\text{Ni-Ti}} = 2.2$ Å and $r_{\text{Ti-Ti}} = 2.75$ Å. To make the simulations we have used the RMC programs and available in the Internet.[9]

The experimental and simulated total structure factors for a-$Ni_{60}Ti_{40}$ alloy are shown in Fig. 5. It can be seen that a very good agreement between them was achieved. The

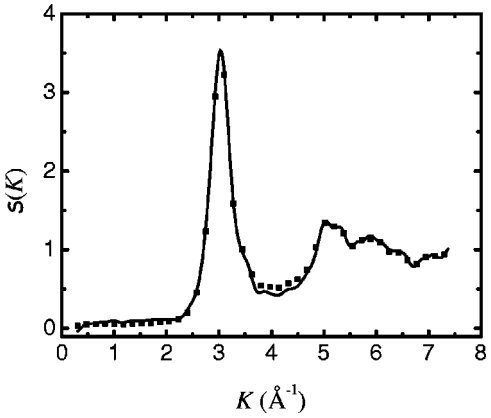

FIG. 5. Experimental (full line) and simulated (squares) total structure factors for a-$Ni_{60}Ti_{40}$ alloy.

$\mathcal{S}^c_{\alpha,\beta}(K)$ factors extracted from the simulation are shown in Fig. 6. In a recent paper, Gazzillo *et al.*[32] reported the $\mathcal{S}_{\text{Ni-Ni}}(K)$, $\mathcal{S}_{\text{Ni-Ti}}(K)$, and $\mathcal{S}_{\text{Ti-Ti}}(K)$ calculated using a nonadditive hard sphere model for amorphous Ni_xTi_{1-x} ($x = 0.3, 0.5, 0.7$) alloys. The $\mathcal{S}^c_{\alpha,\beta}(K)$ factors obtained by us show the same features of those reported (see Fig. 6 of Ref. 32), in particular the pre-peak in $\mathcal{S}_{\text{Ni-Ni}}(K)$ and the shoulder in $\mathcal{S}_{\text{Ti-Ti}}(K)$ located both at about $K = 2$ Å^{-1}.

Figures 7 and 8 show the $G^c_{\alpha,\beta}(r)$ and $\text{RDF}^c_{\alpha,\beta}(r)$ functions, respectively. By using them the coordination numbers and interatomic distances for the first neighbors were obtained and they are displayed in Table I. From EXAFS, the two subshells of Ni-Ni pairs give 8.8 atoms at a mean interatomic distance $\overline{r} = 2.57$ Å, the two subshells of Ni-Ti give

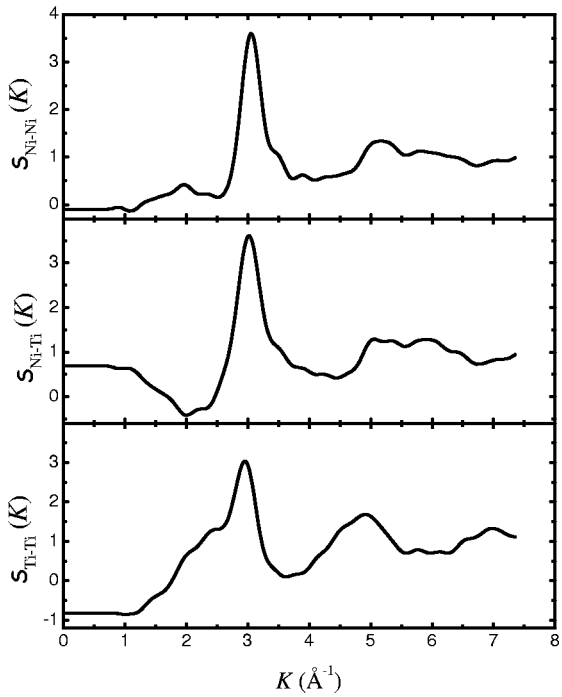

FIG. 6. Calculated partial structure factors $\mathcal{S}^c_{\text{Ni-Ni}}(K)$, $\mathcal{S}^c_{\text{Ni-Ti}}(K)$, and $\mathcal{S}^c_{\text{Ti-Ti}}(K)$ obtained from the RMC simulation for a-$Ni_{60}Ti_{40}$ alloy.

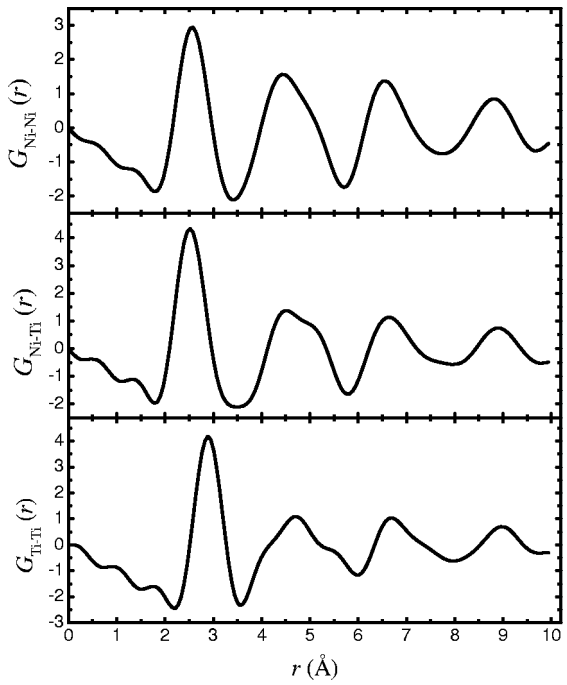

FIG. 7. Calculated partial pair distribution functions $G^c_{\text{Ni-Ni}}(r)$, $G^c_{\text{Ni-Ti}}(r)$, and $G^c_{\text{Ti-Ti}}(r)$ obtained from the RMC simulation for a-$Ni_{60}Ti_{40}$ alloy.

5.2 atoms at a mean interatomic distance $\overline{r}=2.55$ Å while the two subshells of Ti-Ti furnish 5.5 atoms at a mean interatomic distance $\overline{r}=2.90$ Å. By comparing these structural parameters obtained from EXAFS with those found by RMC simulations one can see a good agreement, with exception of

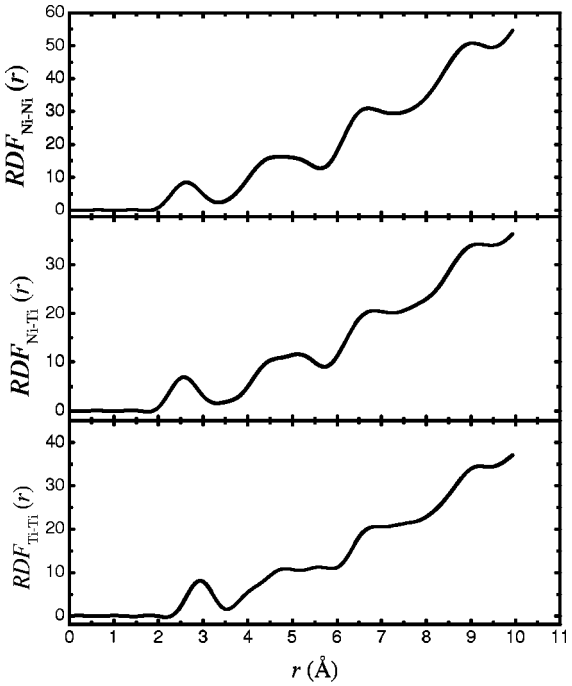

FIG. 8. Calculated partial radial distribuition functions $RDF^c_{\text{Ni-Ni}}(r)$, $RDF^c_{\text{Ni-Ti}}(r)$, and $RDF^c_{\text{Ti-Ti}}(r)$ obtained from the RMC simulation for a-$Ni_{60}Ti_{40}$ alloy.

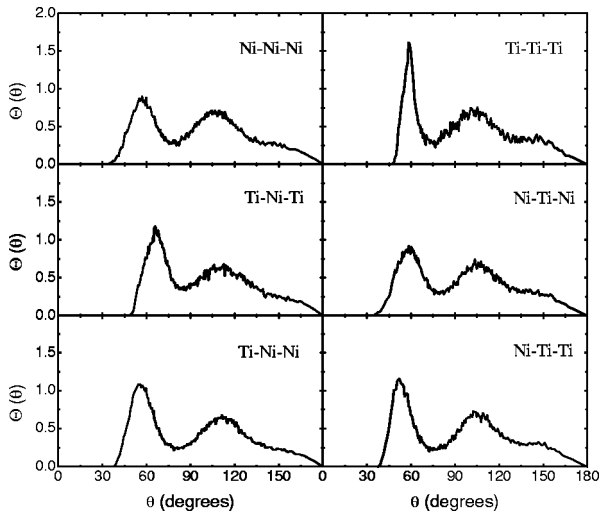

FIG. 9. Calculated partial bond-angle distribution functions $\Theta_{\alpha\text{-}\beta\text{-}\gamma}(\theta)$ for a-$Ni_{60}Ti_{40}$ obtained by using RMC simulations.

the number of Ni-Ni pairs extracted from the EXAFS analysis which is greater than that obtained from RMC simulations.

It should be also noted that the Ni-Ni interatomic distance found by RMC simulations is larger than that one for Ni-Ti pairs. According to Hausleitner and Hafner[33] this is associated with a change of the *d*-band electronic density of states in the Ni-Ti alloys from a common-band to a split-band form. Fukunaga *et al.*[34] have already found Ni-Ti interatomic distances shorter than those for Ni-Ni pairs in the a-$Ni_{40}Ti_{60}$ alloy.

By defining the partial bond-angle distribution functions $\Theta_{\alpha\text{-}\beta\text{-}\gamma}(\theta)$ where β is the atom in the corner, we calculate the angular distribution of the bonds between first neighbor atoms. They were calculated from the final three-dimensional structure obtained from RMC simulation. This kind of information was not obtained from EXAFS analysis because the partial distribution functions extracted from EXAFS give only a one-dimensional description of the atomic arrangement. Fig. 9 shows the six $\Theta_{\alpha\text{-}\beta\text{-}\gamma}(\theta)$ functions found for a-$Ni_{60}Ti_{40}$ alloy. Each $\alpha-\beta-\gamma$ sequence has a maximum around the angles listed in Table II.

In their paper, Hausleitner and Hafner[33] investigated several amorphous alloys formed by transition metals using molecular dynamics simulations. They obtained the structure factors, coordination numbers, interatomic distances, and the bond-angle distribution functions. According to them, if the components of an alloy have a large difference in the number of *d* electrons there is a pronounced non-additivity of the pair interactions and a strong interaction between unlike atoms. These facts favor the formation of trigonal-prismatic units. The bond angle values of triangular and square faces of a distorted prism are found around $\theta=60°$, $90°-100°$.

Ni and Ti atoms have a large difference in the number of *d* electrons in their *d* bands. Figure 9 and the values given in Table II give evidences that the atomic structure of a-$Ni_{60}Ti_{40}$ alloy contains distorted trigonal-prismatic units. The presence of this kind of units was already reported in amorphous $Ni_{33}Ti_{67}$,[11] $Pd_{82}Si_{18}$,[12] and $Ni_{65}B_{35}$[13] alloys.

TABLE II. Angles where each $\Theta_{\alpha\text{-}\beta\text{-}\gamma}(\theta)$ function has a maximum for a-$Ni_{60}Ti_{40}$ alloy.

Bond sequence	Ni-Ni-Ni	Ni-Ti-Ni	Ti-Ni-Ti	Ti-Ti-Ti	Ti-Ni-Ni	Ni-Ti-Ti
θ	57.4	58.5	66.5	58.5	56.0	53.0
(degrees)	107.4	106.0	113.0	103.0	112.4	105.5

In order to compare the coordination numbers and interatomic distances obtained from EXAFS analysis and RMC simulations for a-$Ni_{60}Ti_{40}$ with those found in Ni_3Ti (Ref. 35) and NiTi (Ref. 36) compounds, we have taken their crystallographic data from ICSD database and TAPP software, respectively, and we used them in the software package CRYSTAL OFFICE98[37] to obtain the first-neighbor coordination numbers and interatomic distances. These values are shown in Table I. From this table, it can be seen that the coordination numbers found for the a-$Ni_{60}Ti_{40}$ alloy show are similar to those ones found in the Ni_3Ti compound, with exception of Ti-Ni pairs. In the case of NiTi compound, we observe a reasonable agreement only for the Ti-Ni and Ti-Ti pairs. The a-$Ni_{60}Ti_{40}$ alloy has interatomic distances similar to those ones found in the Ni_3Ti compound, with exception of Ti-Ti pairs. In the case of the NiTi compound, we observe that all interatomic distances are larger than those ones found in the amorphous alloy.

The Ni_3Ti compound is formed by trigonal prismatic units with triangular and square faces ($\theta=60°,109°,120°$ and 180°), rotated two edge-sharing prisms ($\theta=145°$) and high order polyhedral units. The NiTi compound is also formed by trigonal prismatic units with triangular and square faces ($\theta=54°$, 70°, 90°, and 109°). The comparison between the bond-angle distributions found for the a-$Ni_{60}Ti_{40}$ alloy, which is listed in Table II and showed in Fig. 9, and those ones found in the Ni_3Ti and NiTi compounds suggests the presence of the distorted trigonal prismatic units in the structure of the amorphous alloy.

It is interesting to compare the local structures of amorphous $Ni_{60}Ti_{40}$ alloy and Ni_3Ti and NiTi compounds by calculating the Warren chemical short-range order (CSRO) parameter α_1 (Ref. 38)

$$\alpha_1 = 1 - \frac{N_{12}^1}{c_2(c_1 N_2^1 + c_2 N_1^1)}, \tag{7}$$

where $N_1^1 = N_{11} + N_{12}$ and $N_2^1 = N_{22} + N_{21}$ are the total coordination numbers of each species in the first shell. By using the coordination numbers given in Table I, we found $\alpha_1^{\mathrm{EXAFS}} = 0.043$, $\alpha_1^{\mathrm{RMC}} = -0.023$, $\alpha_1^{\mathrm{Ni_3Ti}} = 0.030$ and $\alpha_1^{\mathrm{NiTi}} = -0.143$. The a-$Ni_{60}Ti_{40}$ alloy has a local structure similar to a solid solution, for which $\alpha_1 = 0$, as it happens to the Ni_3Ti compound and different of that found in the NiTi compound.

V. CONCLUSION

The EXAFS technique was used to study the local structure of a-$Ni_{60}Ti_{40}$ alloy produced by MA; the experimental values of the structural parameters agree with those ones extracted from RMC simulations. From the RMC simulations we inferred a three-dimensional structure for a-$Ni_{60}Ti_{40}$ alloy that could not be obtained by EXAFS. The calculated bond-angle distributions suggest that the atomic structure of a-$Ni_{60}Ti_{40}$ contains distorted trigonal prismatic units. The calculated Warren CSRO parameter indicated that the local atomic structure in the a-$Ni_{60}Ti_{40}$ alloy is similar to the one found in a solid solution and there is some resemblance with the one present in the Ni_3Ti compound.

ACKNOWLEDGMENTS

We wish to thank the Conselho Nacional de Desenvolvimento Científico e Tecnológico (CNPq) and Agência Financiadora de Projetos (FINEP) for financial support. We also thank the LNLS staff and, in particular, Dr. A. Y. Ramos for technical support during the EXAFS measurements and data analysis. This work was partially supported by LNLS (Proposal No. XAS 799/01). We thank R. S. de Biasi for suggestions and for a careful reading of the manuscript.

*Electronic address: kleber@fisica.ufsc.br
†Electronic address: fsc1jcd@fisica.ufsc.br

[1] C. Suryanarayana, Prog. Mater. Sci. **46**, 1 (2001).
[2] J.C.D. Lima, E.C. Borba, C. Paduani, V.H.F. dos Santos, T.A. Grandi, H.R. Rechenberg, I. Denicoló, M. Elmassalami, and A.P. Barbosa, J. Alloys Compd. **234**, 43 (1996).
[3] A.W. Weeber and H. Bakker, Physica B **153**, 93 (1988).
[4] D.K. Mukhopadhyay, C. Suryanarayana, and F.H. Froes, Scr. Metall. Mater. **30**, 133 (1994).
[5] A.R. Yavari, P.J. Desré, and T. Benameur, Phys. Rev. Lett. **68**, 2235 (1992).
[6] H. Gleiter, Prog. Mater. Sci. **33**, 223 (1989).
[7] R.L. McGreevy and L. Pusztai, Mol. Simul. **1**, 359 (1988).
[8] R.L. McGreevy, Nucl. Instrum. Methods Phys. Res. A **354**, 1 (1995).
[9] RMCA version 3, R. L. McGreevy, M. A. Howe, and J. D. Wicks, 1993, available at http://www.studsvik.uu.se.
[10] M. Bionducci, G. Navarra, R. Bellisent, G. Concas, and F. Congiu, J. Non-Cryst. Solids **250**, 605 (1999).
[11] E.W. Iparraguirre, J. Sietsma, and B.J. Thijsse, J. Non-Cryst. Solids **156–158**, 969 (1993).
[12] T. Ohkubo, H. Kai, and Y. Hirotsu, Mater. Sci. Eng., A **304–306**, 300 (2001).
[13] L. Pusztai and E. Sváb, J. Phys.: Condens. Matter **5**, 8815 (1993).
[14] J.H. He, H.W. Sheng, P.J. Schilling, C.-L. Chien, and E. Ma,

Phys. Rev. Lett. **86**, 2826 (2001).
[15] T.E. Faber and J.M. Ziman, Philos. Mag. **11**, (1965).
[16] B. Rosi-Schwartz and G. R. Mitchell, Polymer **35**, 5398 (1994).
[17] A. Mellergard and R.L. McGreevy, Acta Crystallogr., Sect. A: Found Crystallogr. **55**, 783 (1999).
[18] L. Karlsson, A. Wannberg, R.L. McGreevy, and D.A. Keen, Phys. Rev. B **61**, 487 (2000).
[19] P. Jóvári and L. Pusztai, Phys. Rev. B **64**, 014205 (2001).
[20] D.A. Keen and R.L. McGreevy, Nature (London) **344**, 423 (1990).
[21] Yuren Wang, Kunguan Lu, and Chenxi Li, Phys. Rev. Lett. **79**, 3664 (1997).
[22] J.D. Wicks and R.L. McGreevy, J. Non-Cryst. Solids **192**, 23 (1995).
[23] A.D. Cicco, M. Taglienti, M. Minicucci, and A. Filipponi, Phys. Rev. B **62**, 12 001 (2000).
[24] C. N. J. Wagner, *Liquid Metals*, edited by S. Z. Beer (Marcel Dekker, New York, 1972), p. 258.
[25] S. Sasaki, *Anomalous Scattering Factors for Synchrotron Radiation Users, Calculated using Cromer and Liberman's Method* (National Laboratory for High Energy Physics, Japan, 1984).
[26] H.C.N. Tolentino, A.Y. Ramos, M.C.M. Alves, R.A. Barrea, E. Tamura, J.C. Cezar, and N. Watanabe, J. Synchrotron Radiat. **8**, 1040 (2001).
[27] D. E. Sayers and B. A. Bunker, *X-ray Absorption: principles, applications, techniques of EXAFS, SEXAFS and XANES* (Wiley-Intersciences, New York, 1988), p. 211.
[28] T. Ressler, J. Phys. IV **7**, C2-269 (1997).
[29] E.A. Stern, D.E. Sayers, and F.W. Lytle, Phys. Rev. B **11**, 4836 (1975).
[30] J.J. Rehr, J. Am. Chem. Soc. **113**, 5135 (1991).
[31] J. C. de Lima, D. M. Trichês, T. A. Grandi, and R. S. de Biasi, J. Non-Cryst. Solids **304**, 174 (2002).
[32] D. Gazzillo, G. Pastore, and S. Enzo, J. Phys.: Condens. Matter **1**, 3469 (1989).
[33] C. Hausleitner and J. Hafner, Phys. Rev. B **45**, 128 (1992).
[34] T. Fukunaga, N. Watanabe, and K. Suzuki, J. Non-Cryst. Solids **61&62**, 343 (1984).
[35] ICSD–Inorganic Crystal Structure Database, Gmchin-Intitut fur Anorganishe Chemie und Fachinformationszentrum FIZ, Karlsruhe, 1995.
[36] TAPP, version 2.2, 1990, E. S. Microware, Inc., 2234 Wade Court, Hamilton, OH 45013.
[37] Atomic Softek, 70 Longwood Road North, Hamilton, Ontario, Canada L8S 3V4.
[38] M. Maret, P. Chieux, P. Hicter, M. Atzmon, and W.L. Jonhson, J. Phys. F: Met. Phys. **17**, 315 (1987).